




Efficient single-photon source based on a deterministically fabricated single quantum dot - microstructure with backside gold mirror

Cite as: Appl. Phys. Lett. **111**, 011106 (2017); <https://doi.org/10.1063/1.4991389>

Submitted: 12 May 2017 . Accepted: 20 June 2017 . Published Online: 05 July 2017

Sarah Fischbach, Arsenty Kaganskiy, Esra Burcu Yazar Tauscher, Fabian Gericke, Alexander Thoma, Ronny Schmidt, André Strittmatter , Tobias Heindel , Sven Rodt, and Stephan Reitzenstein 



View Online



Export Citation



CrossMark

ARTICLES YOU MAY BE INTERESTED IN

[Surface acoustic wave modulation of a coherently driven quantum dot in a pillar microcavity](#)
Applied Physics Letters **111**, 011103 (2017); <https://doi.org/10.1063/1.4990966>

[On-demand generation of background-free single photons from a solid-state source](#)
Applied Physics Letters **112**, 093106 (2018); <https://doi.org/10.1063/1.5020038>

[Single-photon emission at 1.55 \$\mu\text{m}\$ from MOVPE-grown InAs quantum dots on InGaAs/GaAs metamorphic buffers](#)

Applied Physics Letters **111**, 033102 (2017); <https://doi.org/10.1063/1.4993935>

Lock-in Amplifiers
Find out more today



Zurich
Instruments

AIP
Publishing

Efficient single-photon source based on a deterministically fabricated single quantum dot - microstructure with backside gold mirror

Sarah Fischbach, Arseny Kaganskiy, Esra Burcu Yasar Tauscher, Fabian Gericke, Alexander Thoma, Ronny Schmidt, André Strittmatter,^{a)} Tobias Heindel, Sven Rodt, and Stephan Reitzenstein^{b)}

Institut für Festkörperphysik, Technische Universität Berlin, Hardenbergstraße 36, D-10623 Berlin, Germany

(Received 12 May 2017; accepted 20 June 2017; published online 5 July 2017)

We present an efficient broadband single-photon source which is fabricated by a flip-chip gold-bonding technique and *in-situ* electron beam lithography. The device comprises a single InGaAs quantum dot that is centered at the bottom of a monolithic mesa structure and located above a gold mirror for enhanced photon-extraction efficiency. We show a photon-extraction efficiency of $\eta_{ext} = (18 \pm 2)\%$ into a numerical aperture of 0.4 and a high suppression of multi-photon events from this source with $g^{(2)}(0) = 0.015 \pm 0.009$. Our deterministic device with a backside gold mirror can be combined with electrical contacts and piezo-tuning capabilities in future refinements, which represents an important step towards a spectrally tunable plug-and-play quantum-light source with broadband enhancement for photonic quantum networks. *Published by AIP Publishing.*
[\[http://dx.doi.org/10.1063/1.4991389\]](http://dx.doi.org/10.1063/1.4991389)

Applications in the field of photonic quantum technologies rely crucially on the development of bright on-demand single-photon sources (SPSs).¹ One example is secure quantum communication, which is enabled by the exchange of single photons in point-to-point quantum key distribution protocols² and of entangled photon pairs in the more advanced quantum repeater concept.^{3,4} Similarly, basic schemes of quantum computation can be implemented with indistinguishable single photons,⁵ while more complex approaches in linear optical quantum computation operate with entangled photon pairs.⁶ Beyond the optimization of individual quantum light sources, these applications require the controlled fabrication of single-photon and entangled photon-pair sources with high photon-extraction efficiency, high indistinguishability, high entanglement fidelity, and precise spectral tunability to allow, e.g., for entanglement swapping.

Self-assembled semiconductor quantum dots (QDs) in the InGaAs/GaAs material system are excellent single-photon emitters and can also be used for the generation of polarization-entangled photon pairs via the biexciton-exciton radiative cascade.^{7,8} For applications, it is important to enhance their photon-extraction efficiency by integrating them into nanophotonic structures. With microcavities, efficiency values of up to 66% were achieved,⁹ photonic wires gave 72% extraction efficiency,¹⁰ while photonic trumpets served to achieve up to 75%,¹¹ all of them measured at the first collection lens with a numerical aperture of 0.75. In contrast to geometrical approaches, light extraction strategies based on microcavities are very attractive because they enable high extraction efficiencies in compact designs. However, they exhibit a small spectral bandwidth of typically less than 1 nm which makes the spectral matching with

the quantum dot technologically demanding.¹² Furthermore, as a matter of concept, the enhancement of the excitonic as well as the biexcitonic emission is not possible in the same high-finesse microcavity, as the two emission lines show a spectral spread due to the biexciton binding energy.¹³

To achieve high outcoupling efficiencies and a large spectral bandwidth, waveguide approaches¹⁰ and optimized geometrical designs can be utilized, as was recently shown with deterministically fabricated QD microlenses.¹⁴ In this case, a backside mirror is used to direct the emission from an InGaAs QD to the upward direction, while a monolithic microlens is positioned on top to tailor the outcoupling of the upward propagating modes of the structure. The microlens is written by *in-situ* 3D electron-beam lithography (EBL) based on low temperature cathodoluminescence spectroscopy. This method allows one to choose a QD by its spatially and spectrally resolved CL signal and to *in-situ* write a structure on top with EBL.^{14,15} In this way, extraction efficiencies of up to $\eta_{ext}^{0.4} = 29\%$ were realized for an NA of 0.4,¹⁶ along with a large spectral bandwidth of around 10 nm, a high suppression of multi-photon events with $g^{(2)}(0) < 0.01$,¹⁴ and a high degree of photon indistinguishability with $V > 90\%$.¹⁷

So far, this approach was implemented with a distributed Bragg reflector (DBR) acting as a backside mirror, which was integrated during the epitaxial growth of the structure. Implementing a backside gold mirror is, although technologically more challenging, rewarding because of its optical characteristics and additional functionality. First, unlike a DBR, a gold mirror is not limited in its reflection angle. A DBR mirror shows a strong decrease in reflection for incidence angles larger than around 20°. ¹⁸ This issue can be circumvented by a gold mirror to obtain significantly enhanced photon-extraction efficiency at high NAs as we will show below. Moreover, the gold layer can be used as a backside electrical contact, and the used flip-chip goldbonding technique can readily be used to bond the structure onto a piezoelectric actuator for the application of spectral

^{a)}Present address: Otto-von-Guericke Universität Magdeburg, Universitätsplatz 2, D-39106 Magdeburg, Germany.

^{b)}stephan.reitzenstein@physik.tu-berlin.de

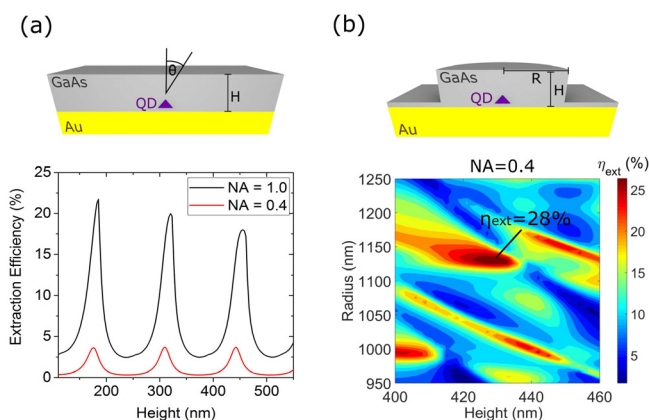


FIG. 1. Numerical simulation of the photon-extraction efficiency at a wavelength $\lambda = 920$ nm from a planar GaAs structure with (a) a backside gold mirror as a function of the slab height and (b) from a mesa structure with a backside gold mirror as a function of height and radius of the structure. The QD is located only 60 nm above the gold mirror.

strain-tuning.¹⁹ Thus, the combination of deterministically written microstructures with backside gold mirrors is an important step towards on-demand, tunable single-photon sources with high extraction efficiency.

The design of our single-photon source was optimized for maximum extraction efficiency at $\lambda = 920$ nm by 3D finite-element simulations using the software package JCMsuite.²⁰ The basic model structure is given by a GaAs layer of variable thickness above a gold mirror [see Fig. 1(a)]. The emitter is located at a distance of 60 nm ($\approx \frac{\lambda}{4n}$) above the mirror to achieve a high emission enhancement by placing it at the antinode of the electromagnetic field. We optimized it to give a high value of the dipole emission subtracted by the amount that was absorbed by the gold layer. In the planar case, our structure works as a Fabry-Pérot cavity, limiting the number of modes in the vicinity of the emitter.²¹ It shows maxima of the extraction efficiency at odd multiples of a lambda-quarter cavity $H = (2m + 1) \times \lambda / (4n)$, $m = 1, 2, \dots$, as the metallic mirror adds another phase shift of π with every roundtrip in the cavity. The number m determines the order of the cavity and the number of resonant modes that exist at different angles θ_m . Only modes which propagate towards the GaAs-air interface with an angle θ_m smaller than the critical angle of total internal reflection $\theta_c = 16.7^\circ$ can be coupled out of the resonator. This leads to a trade-off in the choice of the cavity order: At higher cavity order, more modes exist inside the structure and a fraction of the emission is lost to these modes. At the same time, however, the central angular mode profile with a low value of θ_m is getting smaller with increasing cavity order, which results in a higher directionality of the emission normal to the sample surface.²² Therefore, as shown in Fig. 1(a), the outcoupling to the full upper half-sphere (NA = 1.0) decreases with increasing cavity height, while the maximum emission into an NA of 0.4 remains almost constant at $\eta_{sim}^{0.4} = 3.5\%$. As a trade-off, we choose a third order cavity and suppress the propagation of higher order modes by implementing a lateral confinement with a mesa structure. At the same time, this decreases the mode volume of the upward directed mode, which further increases the coupling with the emitter via the Purcell effect and results in an increased extraction

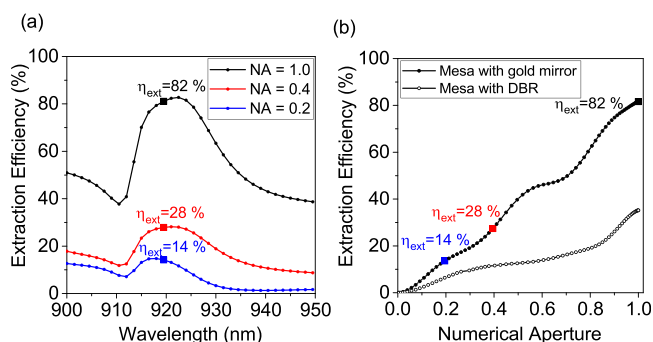


FIG. 2. (a) Calculated photon-extraction efficiency as a function of the emission wavelength of a QD integrated into a mesa structure with a backside gold mirror. The results were determined for three different NAs of the collection optics. (b) Calculated photon extraction efficiency as a function of the NA for a sample structure with a gold mirror (solid circles) and DBR (open circles) optimized for an emitter at $\lambda = 920$ nm.

efficiency. The optimized mesa parameters can be obtained from the parameter scan in Fig. 1(b) and amount to a radius $R = 1130$ nm and height $H = 430$ nm, which leads to a photon-extraction efficiency of $\eta_{sim}^{0.4} = 28\%$. Figure 2(b) shows the extraction efficiency of this structure in comparison to an optimized mesa on top of a DBR mirror depending on the numerical aperture of the collection optics. A significant improvement is observed by the introduction of the gold mirror which increases with the numerical aperture. As mentioned before, this is explained by the limitation of the DBR reflectance by the incidence angle of the light, whereas the reflection by a gold mirror is independent from that angle. Consequently, more light is emitted by the gold mirror especially into large angles when compared to a sample with DBR. This positive impact on the extraction efficiency outnumbers the additional losses that are caused by absorption in the gold layer. Using material properties as given in Ref. 27, we estimated the absorption losses to be 13%. This sets the maximum achievable extraction efficiency at NA = 1 to 87% in the present design which is in quite good agreement with the maximum of 82% of the corresponding curve presented in Fig. 2(b). As demonstrated by a wavelength scan in Fig. 2(a), we achieve a strong enhancement of the emission within a range of $\Delta\lambda \approx 10$ nm, which covers typical biexciton binding energies observed for this material system.¹³

The fabrication of the single-photon source starts with the growth of the layer structure and the InGaAs QDs by metal-organic chemical vapour deposition, followed by a flip-chip gold bonding process to implement the gold mirror and is finalized by the patterning of the microstructure using *in-situ* 3D EBL. During the growth process, an $\text{Al}_{0.97}\text{Ga}_{0.03}\text{As}$ layer with a thickness of $1 \mu\text{m}$ is deposited on a GaAs(001) substrate. This etch-stop layer is followed by 370 nm of GaAs with the QD layer on top. Finally, a top layer with 60 nm of GaAs is grown. For the flip-chip bonding process, 200 nm of gold are deposited onto the sample by electron-beam evaporation. The sample is then placed upside down on another GaAs(001) substrate, which was covered with $2 \mu\text{m}$ of electroplated gold beforehand. To achieve a sufficient cohesion of the two gold layers, thermocompression bonding with a pressure of 6 MPa at a temperature of

320 °C is applied for 6 h. In the next step, the upper GaAs substrate is removed by wet chemical etching, while the lower parts of the sample are protected by a wax coating. A stirred solution of hydrogen peroxide and ammonium hydroxide is used as an etching agent until the process is stopped by the $\text{Al}_{0.97}\text{Ga}_{0.03}\text{As}$ layer. The latter is removed by hydrochloric acid, and the gold-bonded semiconductor membrane with a thickness of only 430 nm remains. The sample is released from the wax and ready to be processed by *in-situ* EBL. For the lithography step, the sample is spin-coated with the electron-beam resist AR-P 6200 (CSAR 62)²³ and transferred into a customized scanning electron microscope for CL spectroscopy and *in-situ* EBL at cryogenic temperatures (for further information on the setup, see Ref. 24). Areas of $20\ \mu\text{m} \times 20\ \mu\text{m}$ on the sample are mapped at a temperature of $T = 5\ \text{K}$. Next, a QD with high brightness at the desired wavelength is chosen and a mesa is written into the resist on top of it. Afterwards, the resist is developed and the structure is transferred into the GaAs top layer by reactivation-enhanced plasma etching (for details, see Ref. 23).

To characterize the single-photon emission of our device, it is placed in a micro-photoluminescence (μPL) setup which allows for Hanbury-Brown and Twiss (HBT) measurements. The sample is cooled down to 10 K inside a liquid-helium flow cryostat. For time-integrated measurements, it is optically excited by a continuous wave laser at 671 nm. The luminescence is collected by an objective with an NA of 0.4, spectrally dispersed by a monochromator and detected with a Si-based charge-coupled device camera (spectral resolution of $25\ \mu\text{eV}$). A map scan of the collected photoluminescence is shown in Fig. 3. The image visualizes the much stronger emission from two QD-mesas as compared to the emission from QDs in the surrounding unprocessed planar area. QD-mesa 1 features a bright emission line at 918 nm and a second line at 920 nm, as shown in Fig. 4(a), which are identified as the exciton (X) and the biexciton (XX) emission lines according to their excitation power dependent intensities [see Fig. 4(b)].

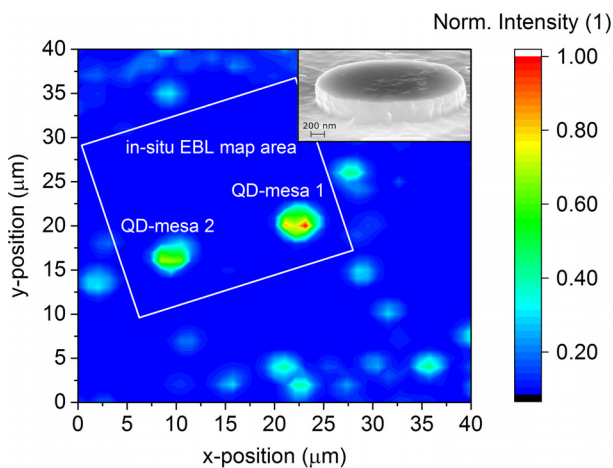


FIG. 3. μPL map of two mesa structures within an *in-situ* EBL processed area where all other QDs are etched away. Outside the *in-situ* EBL map area emission from other, much dimmer QDs in the unprocessed planar region are visible for comparison. The inset displays an SEM image of QD-mesa 1.

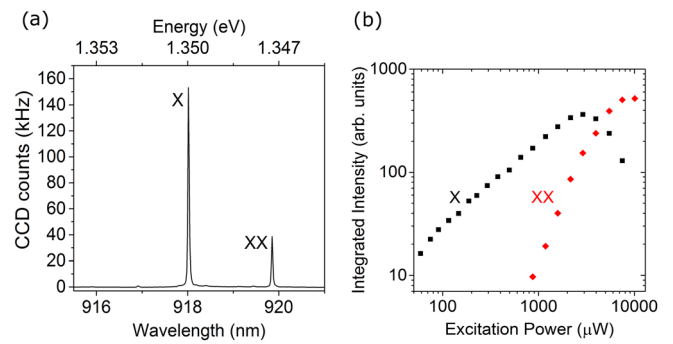


FIG. 4. (a) μPL spectrum of a QD-mesa structure. (b) The QD emission lines can be identified to originate from the transition of an exciton and a biexciton according to their excitation power dependence.

In order to determine the photon-extraction efficiency, the device is excited by a pulsed Ti:Sapphire laser ($f = 80\ \text{MHz}$) at saturation of the X emission with an excitation power $P = 166\ \mu\text{W}$ at a wavelength of $\lambda = 889\ \text{nm}$ (corresponding to wetting layer excitation). To measure the extraction efficiency of the single-photon emission, we determined the setup efficiency as described in Ref. 14 to $\eta_{\text{setup}} = 0.9\%$ and measured the count-rate of the X emission at saturation using single-photon counting modules. The observed efficiency amounts to $\eta_{\text{ext}} = (18 \pm 2)\%$. The deviation from the theoretically estimated value of $\eta_{\text{sim}}^{0.4} = 28\%$ can be explained by processing tolerances as follows: First, the positioning accuracy of the *in-situ* EBL method has been determined to be $34\ \text{nm}$.²⁴ Second, we estimate deviations of $\Delta R = \pm 50\ \text{nm}$ and $\Delta H = \pm 10\ \text{nm}$ in the radius and the height of the mesa due to variations in the anisotropic and isotropic impact of the dry etching step. As visible in Fig. 1(b), these tolerances have a significant impact on the optical performance and can reduce the achievable photon-extraction efficiency as observed in the experiment. Further numerical optimizations will focus on more tolerant designs to achieve optimum photon-extraction efficiency also under experimental conditions.

To prove the quantum nature of the emission from our device, we measured the second-order photon-autocorrelation function. In our measurement setup, the signal can be redirected to a second monochromator exit that couples into a Hanbury-Brown and Twiss setup with an overall timing resolution of 350 ps. The results are given in Fig. 5 and show a clear antibunching at $\tau = 0$. To determine the $g^{(2)}(0)$ value, the following relation²⁵ was fitted to the data:

$$g^{(2)}(\tau) = \left(g^{(2)}(0) \times e^{\frac{-|\tau|}{\tau_{sp}}} + \sum_{n \neq 0} e^{\frac{-|\tau - n\tau_{sp}|}{\tau_{sp}}} \right) * G_s(\tau_s), \quad (1)$$

with a pulse separation of τ_p and a Gaussian distribution $G_s(\tau_s)$ to account for the timing resolution of the setup of $\tau_s = 350\ \text{ps}$. We gain an estimate for the spontaneous lifetime of the transition of $\tau_{sp} = (0.58 \pm 0.10)\ \text{ns}$ and a value of the antibunching of $g^{(2)}(0) = 0.015 \pm 0.009$, which demonstrates an almost perfect single-photon emission from the QD-mesa structure.

In conclusion, we have shown that we can realize a broadband single-photon source with a high suppression of

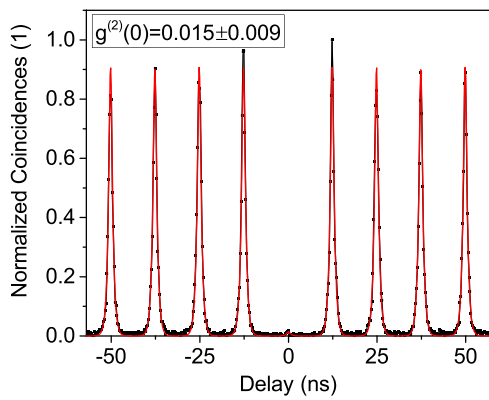


FIG. 5. Measurement of the second-order photon-autocorrelation of the X-emission of the deterministic QD-mesa 1 with a backside gold mirror [see Fig. 4(a)] recorded at saturation of the X emission. The black dots are experimental data and the red line results from curve fitting as explained in the text.

multi-photon events and a photon-extraction efficiency of $\eta_{ext}^{0.4} = (18 \pm 2) \%$ by combining deterministic processing of QD microstructures with a backside gold mirror. We see high potential for further optimization of the light outcoupling by the structuring of microlenses instead of mesa structures or by the introduction of a dielectric layer above the gold mirror to decrease the absorption.²⁹ In this context, we would like to point out that performing 3D *in-situ* EBL on a sample with a backside gold mirror is more demanding as compared to a sample with a backside DBR mirror, because the resist contrast is higher, which results in a smaller dose window for the writing process of a microlens. Besides that, the collection of emission with high numerical apertures can give results of $\eta_{ext} = 70\% - 80\%$. In this respect, the integration of high-NA multi-lens micro-objectives written with femtosecond 3D direct laser writing^{26,28} is very promising. The presented approach with a backside gold mirror will be beneficial for the realization of efficient and electrically driven SPSs, as the gold layer can readily be used as a backside electrical contact. Moreover, during the flip-chip bonding process, the structure can be attached to a piezoelectric actuator, which will allow for a piezo-tuning of the emission.

We acknowledge support from project EMPIR 14IND05 MIQC2 (the EMPIR initiative is co-funded by the European Union's Horizon 2020 research and innovation programme and the EMPIR Participating States) and from Deutsche Forschungsgemeinschaft (DFG) through SFB 787 "Semiconductor Nanophotonics: Materials, Models, Devices," as well as from the German Federal Ministry of

Education and Research (BMBF) through the VIP-project QSOURCE (Grant No. 03V0630).

¹G. J. Milburn, *Phys. Scr.* **2009**, 014003.

²C. H. Bennett and G. Brassard, in Proceedings of the IEEE International Conference on Computers, Systems and Signal Processing (1984), p. 175.

³A. K. Ekert, *Phys. Rev. Lett.* **67**, 661 (1991).

⁴N. Gisin and R. Thew, *Nat. Photonics* **1**, 165 (2007).

⁵S. Aaronson and A. Arkhipov, *Theory Comput.* **9**, 143 (2013).

⁶E. Knill, R. Laflamme, and G. J. Milburn, *Nature* **409**, 46 (2001).

⁷O. Benson, C. Santori, M. Pelton, and Y. Yamamoto, *Phys. Rev. Lett.* **84**, 2513 (2000).

⁸N. Akopian, N. H. Lindner, E. Poem, Y. Berlatzky, J. Avron, D. Gershoni, B. D. Gerardot, and P. M. Petroff, *Phys. Rev. Lett.* **96**, 130501 (2006).

⁹X. Ding, Y. He, Z.-C. Duan, N. Gregersen, M.-C. Chen, S. Unsleber, S. Maier, C. Schneider, M. Kamp, S. Höfling, C. Lu, and J.-W. Pan, *Phys. Rev. Lett.* **116**, 020401 (2016).

¹⁰J. Claudon, J. Bleuse, N. S. Malik, M. Bazin, P. Jaffrennou, N. Gregersen, C. Sauvan, P. Lalanne, and J.-M. Gerard, *Nat. Photonics* **4**, 174 (2010).

¹¹M. Munsch, N. S. Malik, E. Dupuy, A. Delga, J. Bleuse, J.-M. Gérard, J. Claudon, N. Gregersen, and J. Mørk, *Phys. Rev. Lett.* **110**, 177402 (2013).

¹²A. K. Nowak, S. L. Portalupi, V. Giesz, O. Gazzano, C. Dal Savio, P.-F. Braun, K. Karrai, C. Arnold, L. Lanco, I. Sagnes, A. Lemaître, and P. Senellart, *Nat. Commun.* **5**, 3240 (2014).

¹³S. Rodt, A. Schliwa, K. Pötschke, F. Guffarth, and D. Bimberg, *Phys. Rev. B* **71**, 155325 (2005).

¹⁴M. Gschrey, A. Thoma, P. Schnauber, M. Seifried, R. Schmidt, B. Wohlfeil, L. Krüger, J. H. Schulze, T. Heindel, S. Burger, F. Schmidt, A. Strittmatter, S. Rodt, and S. Reitzenstein, *Nat. Commun.* **6**, 7662 (2015).

¹⁵M. Gschrey, F. Gericke, A. Schüssler, R. Schmidt, J.-H. Schulze, T. Heindel, S. Rodt, A. Strittmatter, and S. Reitzenstein, *Appl. Phys. Lett.* **102**, 251113 (2013).

¹⁶A. Schlehahn, M. Gaafar, M. Vaupel, M. Gschrey, P. Schnauber, J.-H. Schulze, S. Rodt, A. Strittmatter, W. Stolz, A. Rahimi-Iman, T. Heindel, M. Koch, and S. Reitzenstein, *Appl. Phys. Lett.* **107**, 041105 (2015).

¹⁷A. Thoma, P. Schnauber, M. Gschrey, M. Seifried, J. Wolters, J.-H. Schulze, A. Strittmatter, S. Rodt, A. Carmele, A. Knorr, T. Heindel, and S. Reitzenstein, *Phys. Rev. Lett.* **116**, 033601 (2016).

¹⁸T. Gessmann and E. F. Schubert, *J. Appl. Phys.* **95**, 2203 (2004).

¹⁹R. Trotta, P. Atkinson, J. D. Plumhof, E. Zallo, R. O. Rezaev, S. Kumar, S. Baunack, J. R. Schröter, A. Rastelli, and O. G. Schmidt, *Adv. Mater.* **24**, 2668 (2012).

²⁰See <http://jcmwave.com> for JCMSuite, JCMwave GmbH.

²¹W. Barnes, G. Björk, J. Gérard, P. Jonsson, J. Wasey, P. Worthing, and V. Zwiller, *Eur. Phys. J. D* **18**, 197 (2002).

²²H. Benisty, H. D. Neve, and C. Weisbuch, *IEEE J. Quantum Electron.* **34**, 1612 (1998).

²³A. Kaganskiy, T. Heuser, R. Schmidt, S. Rodt, and S. Reitzenstein, *J. Vac. Sci. Technol. B* **34**, 061603 (2016).

²⁴M. Gschrey, R. Schmidt, J.-H. Schulze, A. Strittmatter, S. Rodt, and S. Reitzenstein, *J. Vac. Sci. Technol. B* **33**, 021603 (2015).

²⁵H. Nakajima, S. Ekuni, H. Kumano, Y. Idutsu, S. Miyamura, D. Kato, S. Ida, H. Sasakura, and I. Suemune, *Phys. Status Solidi C* **8**, 337 (2011).

²⁶N. Gregersen, T. R. Nielsen, J. Mørk, J. Claudon, and J.-M. Gérard, *Opt. Express* **18**, 21204 (2010).

²⁷K. M. McPeak, S. V. Jayanti, S. J. P. Kress, S. Meyer, S. Iotti, A. Rossinelli, and D. J. Norris, *ACS Photonics* **2**, 326 (2015).

²⁸S. Fischbach, A. Schlehahn, A. Thoma, N. Srocka, T. Gissibl, S. Ristok, S. Thiele, A. Kaganskiy, A. Strittmatter, T. Heindel, S. Rodt, A. Herkommer, H. Giessen, and S. Reitzenstein, *ACS Photonics* **4**, 1327 (2017).

²⁹T. Gissibl, S. Thiele, A. Herkommer, and H. Giessen, *Nat. Photonics* **10**, 554 (2016).